

Crystal plasticity finite element analysis of linear and non-linear extrusion processes

ŞİMŞEK Üİke^{1,a}, MIYAMOTO Hiroyuki^{2,b} and YALÇINKAYA Tuncay^{1,c*}

¹Department of Aerospace Engineering, Middle East Technical University, Ankara, 06800, Türkiye

² Department of Mechanical Engineering, Doshisha University, Kyoto, 610-0321, Japan

^aulke.simsek@metu.edu.tr, ^bhmiyamot@mail.doshisha.ac.jp, ^cyalcinka@metu.edu.tr

Keywords: Crystal Plasticity, Twist Extrusion, Severe Plastic Deformation

Abstract. Severe plastic deformation (SPD) induced by conventional forming processes such as extrusion has a significant effect on texture evolution and strength of metals. Conventional twist extrusion (TE) process can be used to produce ultra-fine grained (UFG) structures without introducing any significant change in the overall dimensions of the sample. However, the commercialization for industrial usage has been limited because of production efficiency and non-uniform distribution of grain refinements. In order to overcome these difficulties a new process called nonlinear twist extrusion (NLTE) has been introduced recently where TE mold channel is modified to restrain strain reversal and rigid body rotation of the workpiece. Prediction of the texture evolution in these processes is crucial for mold design and process parameters. In this work, the texture evolution during NLTE and TE processes are investigated through crystal plasticity finite element method. Single copper crystal which has a billet form is fully extruded through the TE and NLTE mold models separately. In addition to spatial stress and strain evolution investigations, the orientation differences and texture evolution of extruded billets are examined for two different initial orientations of single copper crystal. Moreover, the deformation histories at different locations of the sample are analyzed with crystal plasticity finite element method (CPFEM) to compare the performance of both techniques.

Introduction

Severe Plastic Deformation (SPD) is an efficient manufacturing technique to produce ultrafine-grained (UFG) structures with high densities of lattice defects. In recent years, SPD methods have been popular with their capability for refining the grain size of materials to sub-micrometer and nanometer scales [1]. The strength and resistance to the plastic flow of polycrystalline materials depend on the grain size. Usually, UFG materials have several advantages compared to coarse-grained counterparts with their high strength and other superior properties, including potential use in super-plastic forming operations at elevated temperatures [2]. Various early reports describe interesting results from different SPD techniques to produce UFG structured materials. Equal channel angular pressing (ECAP) (see e.g. [3]), high-pressure torsion (HPT) (see e.g. [4]), accumulated roll bonding (ARB) (see e.g. [5]), multi-directional forging (MDF) (see e.g. [6]), and twist extrusion (TE) (see e.g. [7]) can be listed as the most popular SPD processes. All these methods have certain advantages and disadvantages compared to each other. ECAP process has some operational difficulties and produces excessive waste compared to the other SPD processes. A potential problem in HPT processing is the strain which varies across the disk specimen. Besides, HPT and ECAP processes do not apply to large bulk materials. ARB process also suffers in-homogeneity of strain distribution, and it requires multi-passes. The grain refinement ability of MDF is lower than all other SPD processes, and grain size reduction is not homogenous through the center of the sample. TE process has in-homogenous distribution characteristics, and strain

distribution increases from the center to the periphery. It also requires multi-passes to increase the homogeneous distribution of grains through the workpiece.

In SPD processing, UFG formation is facilitated in deformation routes that involve high dislocation accumulation, and strain reversal or redundant strain reduces the rate of the dislocation accumulations and hence retard the UFG formation. Therefore, the non-linear twist extrusion (NLTE) technique has recently been developed by the authors (see [8]) based on TE, aiming to avoid strain reversal and rigid body rotation, which retard the UFG formation. Numerical analysis of the NLTE process shows the advantages of this process in terms of punching force and deformation distribution.

The numerical modeling of texture evolution during SPD techniques is crucial for understanding the grain refinement mechanisms. The results can be used for optimizing the process and mold parameters for SPD methodology. Nowadays, the crystal plasticity finite element method (CPFEM) is an effective tool for simulating texture evolution during SPD. In recent years, CPFEM simulations of some SPD methods have been performed in various studies. For example, the capability of the CPFE approach in predicting texture formed during ECAP and deformation heterogeneity of single crystal materials were examined (see e.g. [9]). The deformation history and texture evolution during TE were investigated (see e.g. [10]). Crystallographic texture evolution in simple shear extrusion (SSE) process was compared with experimental results (see e.g. [11]). Coupling of FEM flow and crystal plasticity simulations were conducted during the helical extrusion process (see e.g. [12]).

In this study, a single copper crystal with a billet form is fully extruded through the TE and NLTE mold models separately. In addition to spatial stress and strain evolution investigations, the orientation differences and texture evolution of extruded billets are examined for two different initial orientations of single copper crystal, i.e. $\langle 111 \rangle$ and $\langle 100 \rangle$ using crystal plasticity finite element technique. Moreover, the deformation histories at different locations of the sample are analyzed to compare the performance of both methods.

Finite Element Models

Fig. 1 shows the Abaqus finite element models of the twist extrusion processes. In the LTE process, a billet is pressed through a die with two straight channels separated by a section with helical geometry. Apart from being continually rotated in the helical part of the die, a cross-section of the billet normal to the extrusion axis stays unchanged during its translational movement. The mold model of LTE and punch are considered rigid bodies in CPFEM simulations. Encastrate boundary conditions ($u_1=u_2=u_3=R_1=R_2=R_3=0$) were applied through mold geometry from its rigid body reference point (center of mass). Velocity boundary conditions (2 mm/s) were applied through punch rigid body reference point (center of mass). Similarly, the model for NLTE is also presented in Fig. 1.

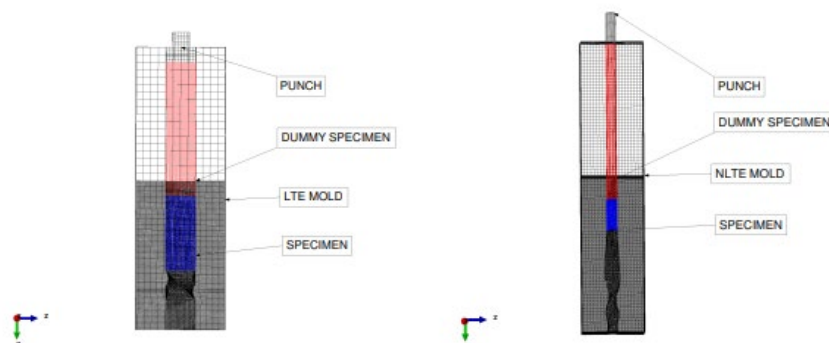


Fig. 1. LTE (left) and NLTE (right) processes FEM model.

Table 1. FEM model mesh parameters of simulated LTE and NLTE processes.

Model	Element Type	Element Family	Number of Elements
LTE Mold	Implicit-Tetrahedral-C3D4-Rigid	3D Stress	33777765
LTE Punch	Implicit-Hexahedral-C3D8R	3D Stress	925
LTE Specimen	Implicit-Hexahedral-C3D8R	3D Stress	159989
NLTE Mold	Implicit-Tetrahedral-C3D4-Rigid	3D Stress	419316
NLTE Punch	Implicit-Hexahedral-C3D8R	3D Stress	1679
NLTE Specimen	Implicit-Hexahedral-C3D8R	3D Stress	48750

The significant difference from LTE is that the billet is extruded, keeping rotation around the longitudinal axis so that the strain reversal is avoided. The mold model of NLTE and punch are considered rigid bodies. Boundary conditions are applied to the model same as in LTE simulations. Single copper crystal specimens are modeled with square and cylindrical shapes for LTE and NLTE, respectively. The square specimen dimensions were 20mm × 20mm × 50mm, and the dimensions of the cylindrical specimen were 20mm r = 10mm×30mm. Mesh properties of SPD models are presented in Table 1.

Crystal Plasticity Constitutive Model

This study utilizes a modified version of a crystal plasticity framework implemented as a UMAT (user-defined material model) subroutine [13]. In the classical crystal plasticity theory, the deformation gradient tensor \mathbf{F} is multiplicatively decomposed into an elastic component \mathbf{F}^e and a plastic component \mathbf{F}^P [14] according to

$$\mathbf{F} = \mathbf{F}^e \mathbf{F}^P \quad (1)$$

According to Schmidt’s Law, the resolved shear stress (τ^α) on a slip system is the leading cause of dislocation slip [15], which can be calculated by,

$$\tau^\alpha = \boldsymbol{\sigma} : \mathbf{s}^{*\alpha} \otimes \mathbf{m}^{*\alpha} \quad (2)$$

In Eq. 2, $\boldsymbol{\sigma}$ is the Cauchy stress tensor is projected on the slip systems where $\mathbf{m}^{*\alpha}$ and $\mathbf{s}^{*\alpha}$ are the slip direction and normal to slip plane in the current configuration, and α represents the slip system number. \mathbf{m}^α and \mathbf{s}^α are in the reference configuration,

$$\mathbf{s}^{*\alpha} = \mathbf{F}^e \mathbf{s}^\alpha \quad (3)$$

$$\mathbf{m}^{*\alpha} = \mathbf{m}^\alpha \mathbf{F}^{e-1} \quad (4)$$

The plastic velocity gradient, \mathbf{L}^P is calculated by,

$$\dot{\mathbf{F}}^P \mathbf{F}^{P-1} = \mathbf{L}^P = \sum_{\alpha=1}^n \dot{\gamma}^\alpha \mathbf{s}^\alpha \otimes \mathbf{m}^\alpha \quad (5)$$

The power law type rate-dependent formulation, which relates the slip rate on each slip system to the resolved shear stress τ^α and the slip resistance g^α is given in Eq. 6

$$\dot{\gamma}^\alpha = \dot{\gamma}_0 \text{sign}(\tau^\alpha) \left| \frac{\tau^\alpha}{g^\alpha} \right|^n \quad (6)$$

where $\dot{\gamma}_0$ is the reference shear strain rate, and n is the rate sensitivity parameter. The slip resistance g^α is calculated considering the latent hardening as presented below. The hardening moduli $h^{\alpha\beta}$ gives the rate of strain hardening on slip system α due to slip system β . The occurrence of self and latent hardening is phenomenologically described by Eq. 8, with q representing latent hardening matrix.

$$\dot{g}^\alpha = \sum_{k=1}^{12} h^{\alpha\beta} |\dot{\gamma}^\beta| \tag{7}$$

$$h^{\alpha\beta} = q^{\alpha\beta} h^{\alpha\alpha}(\gamma) \tag{8}$$

Pierce, Asaro, and Needleman [16] have used a simple form for the self-hardening moduli,

$$h_{\alpha\alpha} = h(\gamma) = h_0 \operatorname{sech}^2 \left| \frac{h_0 \gamma}{g_s - g_0} \right| \tag{9}$$

where h_0 is the initial hardening modulus, g_s is the stage I stress, and γ is the Taylor cumulative shear strain on all slip systems in Eq. 10.

$$\gamma = \sum_{\alpha} \int_0^t |\dot{\gamma}^\alpha| dt \tag{10}$$

In the literature, there is a lot of inconsistent experimental data for single-crystal copper tension tests. Therefore, pure copper polycrystalline stress-strain data under tensile tests are used to calibrate single-crystal copper mechanical properties through homogenization. Symmetric boundary conditions are applied to representative volume element (RVE) cube composed of 500 hundred randomly oriented grains. RVE cube is illustrated in Fig. 2. Data and homogenization curve are illustrated in Fig. 3. The Parameters of a single copper crystal are given in Table 2.



Fig. 2. 500 grained calibration cube model for homogenization.

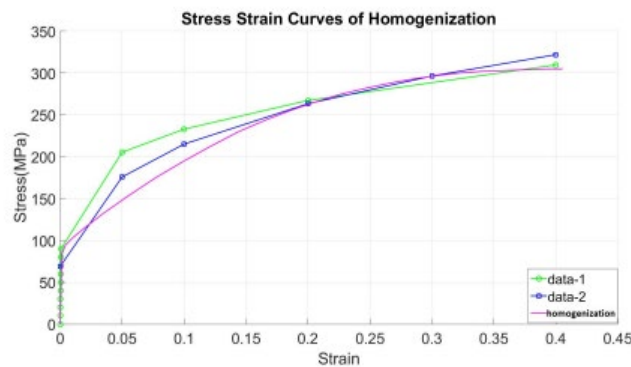


Fig. 3. Homogenization curve vs. data [17].

Table 2. Single crystal copper UMAT material model parameters.

Model	C_{11}	C_{12}	C_{44}	g_0	g_s	h_0	$\dot{\gamma}_0$	n	q
UMAT	168000	121400	75400	25	115	120	0.001	17	1.4

CPFEM Simulation Results

Finite element simulations of LTE and NLTE processes are performed for initially <100> and <111> oriented single copper specimens. The simulations illustrate an initial quadratic increase of the load in LTE and NLTE processes when the specimen head enters the twist zone. After the sudden increase, the slope of the curve starts to decrease, and the punch force slightly increases throughout both processes. The required punch force is less than the LTE process for the NLTE process (Fig.4). This is one of the prominent advantages of NLTE. Black curves show the initially <111> oriented single copper crystal results, and green curves show the initially <100> oriented single copper crystal simulation results. In the LTE process, initially <100> oriented single copper crystal faces with more punch force compared to initially <111> oriented single copper crystal. On the contrary, in the NLTE process, initially <111> oriented single copper crystal needs more punch force throughout the process. Since the cross-section areas are different for both cases, punch pressures are compared for a better presentation. However, the punch forces are dependent on the frictional coefficient. In these calculations, the friction coefficient is set to be low (less than 0.01) due to the convergence problems of implicit solver in contact non-linearities and frictional discontinuities. If the friction coefficient increases, the punch forces will also increase for both processes. The sharp increase in the LTE case is due to the sudden change in the cross-section, which does not exist in the proposed smoother non-linear process.

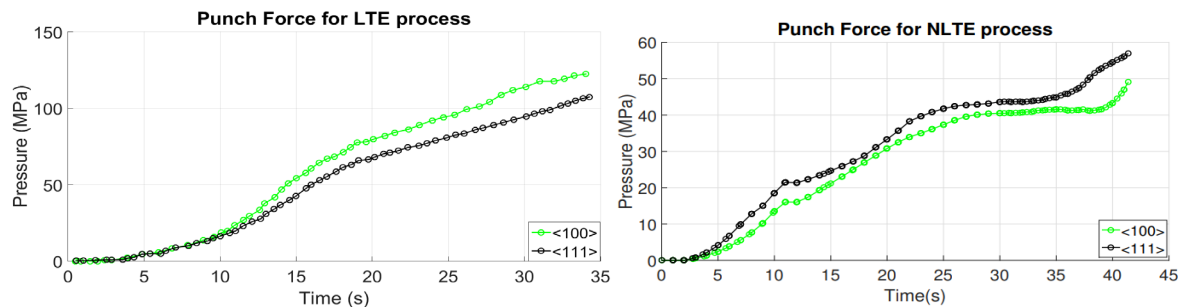


Fig. 4. LTE and NLTE processes punch forces according to the single-crystal copper initial orientation.

Von Mises stress contours are illustrated in Fig. 5 and Fig.6 for LTE and NLTE processes for initially <100> oriented single copper crystal, respectively. The stress values show an increase from the specimen center to the periphery, and maximum stresses can be observed at the edge of the surfaces. In the LTE process, stress evolution is more heterogeneous, and higher stress values are obtained in periphery regions. On the contrary, in the NLTE process, the stress distribution is more homogenous, and high-stress values are inspected in the periphery region and throughout the single copper specimen.

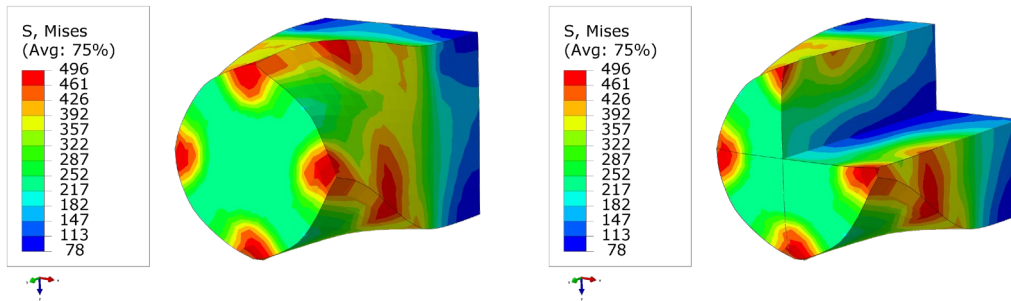


Fig. 5. Von Mises stress (MPa) results of $\langle 100 \rangle$ oriented copper single crystal after one pass of LTE (left) with section view (right).

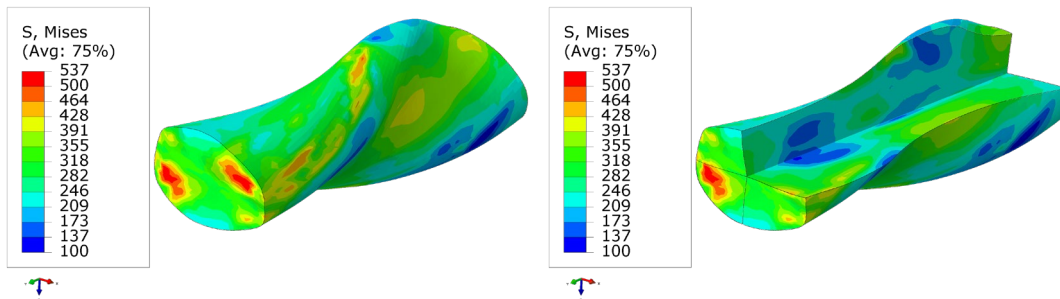


Fig. 6. Von Mises stress (MPa) results of $\langle 100 \rangle$ oriented copper single crystal after one pass of NLTE (left) with section view (right).

Fig. 7 and Fig.8 show the equivalent plastic strain distribution in LTE and NLTE processes, for initially $\langle 111 \rangle$ oriented single copper crystal, respectively. In the LTE process, a smaller magnitude of equivalent plastic strain evolves around the specimen center, and there is a gradual increase from the center to the surface of the specimen for both initial conditions. Distinctively, in the NLTE process, equivalent plastic strain evolves uniformly. Equivalent plastic strain distributions are more homogenous in the center when compared to the periphery region. Single copper crystal is subjected to much more plastic equivalent strain during the NLTE process. To show the deformation characteristics of LTE and NLTE processes, two typical elements of workpieces were chosen at the center and the periphery sections of the specimen distinctively. The selected elements are highlighted in Fig. 9.

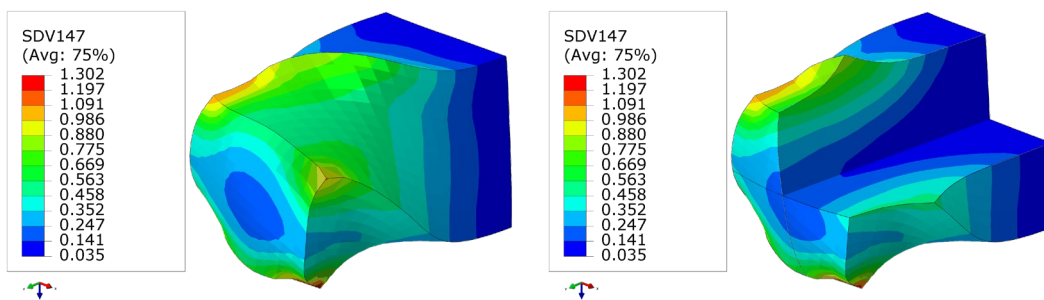


Fig. 7. Plastic equivalent strain results of $\langle 111 \rangle$ oriented copper single crystal after one pass of LTE process (left) with their section view (right).

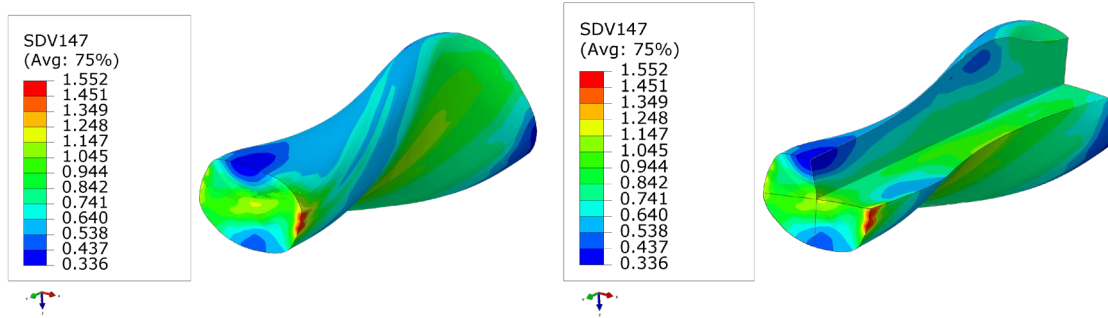


Fig. 8. Plastic equivalent strain results of $\langle 111 \rangle$ oriented copper single crystal after one pass of NLTE process (left) with their section view (right).

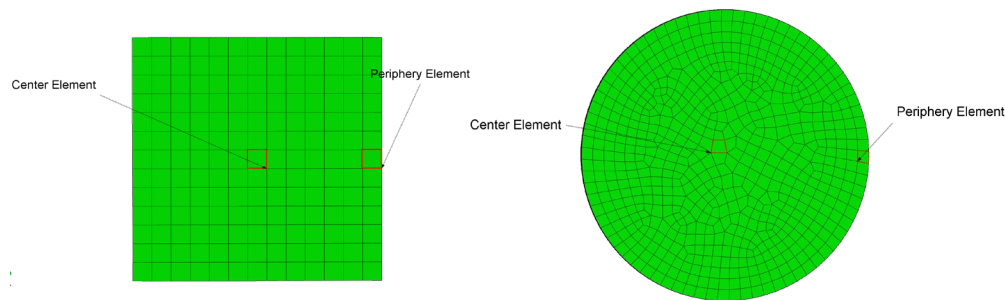
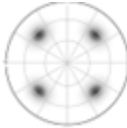
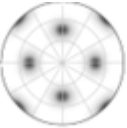
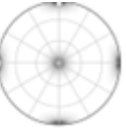
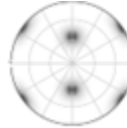
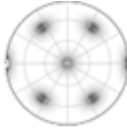

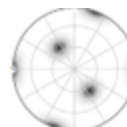
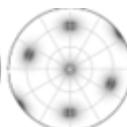
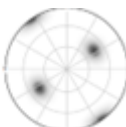
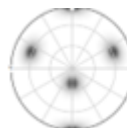

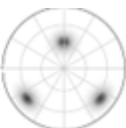
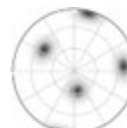
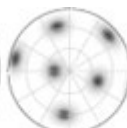
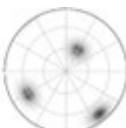


Fig. 9. Investigated elements with their local coordinates at the center and the middle for LTE process (left) and the NLTE process (right).

Certain texture components of face-centered cubic (FCC) materials assist in understanding the final texture of a single copper crystal after deformation. Table 3 pole figures show the main texture components of FCC materials: Copper, Brass, Goss, and S orientations. It gives information about mechanical behaviors and physical and chemical properties of materials and is associated with the performance in their production and investigation in engineering applications. Hence, an accurate understanding of deformation mechanisms and precise control of texture evolution becomes a requirement for developing new materials [18].

Table 3. Texture components and pole figures for face centered cubic (FCC) materials according to [111], [110] and [100] plane respectively [19].

Components Name	Directions	Bunge Euler Angles (ZXZ)	Pole Figures of Components		
			[111]	[110]	[100]
Cube	[001]<100>	0° 0° 0°			
Goss	[011]<100>	0° 45° 0°			
Brass	[0-11]<211>	35° 45° 0°			
Copper	[-211]<111>	90° 35° 45°			
S	[111]<110>	60° 32° 65°			

FCC materials with high or medium stacking fault energy (SFE) grains tend to rotate toward the copper-type textures with increasing deformation, and dislocation slip has been recognized as the dominant deformation mechanism during the whole deformation stage. SFE plays an essential role in determining the dominant mechanisms of plastic deformation. In metals with high SFE (e.g., aluminum and copper), slip is the dominant deformation mode, and the rolling texture is composed of copper, brass, and S texture components. In materials with low SFE, the copper-oriented grains cluster at the prior deformation stage. However, with increasing loading, these grains rotate to the brass-type textures, and the latter dominates in the final textures' at large deformations. The rolling texture in these metals is known as alloy-type texture and is composed of a strong brass component and a minor Goss orientation [20]. After the first pass of LTE and NLTE processes, results for the center and periphery elements are illustrated in Fig.10, respectively. The initial orientation distributions significantly change by the processes for one pass. The distribution of the orientations in pole figures after the LTE and NLTE processes resemble the main orientation pole figures of copper and s textures orientation distributions. Thus, the pole figures of NLTE and LTE processes show that the elements of the single copper specimen face shear deformation during both processes, and their dominant deformation is dislocation slip. Moreover, after one pass, the center and periphery elements' orientation distributions are very close in the NLTE process compared to the LTE process.

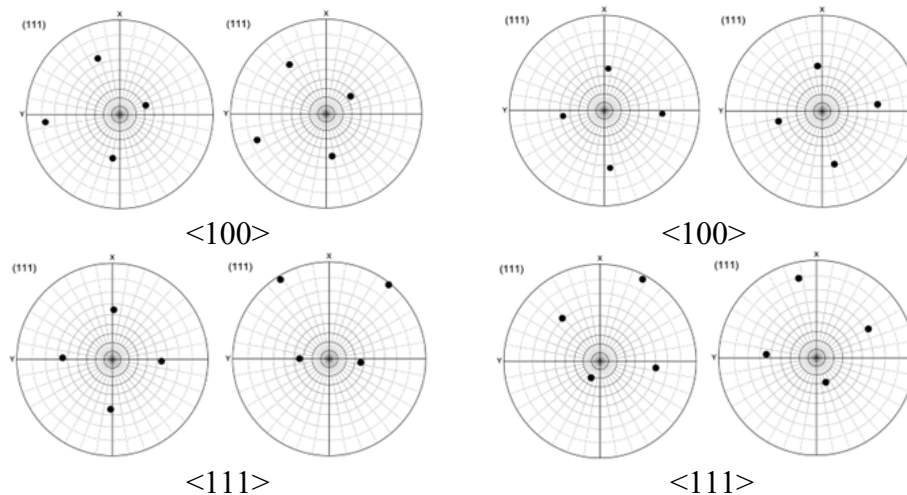


Fig. 10. Pole figures of center (left) and periphery (right) elements of single crystal copper specimen after LTE process according to the initial orientations (<100> and <111>) (Left) and pole figures of center (left) and periphery (right) elements of single crystal copper specimen after NLTE process according to the initial orientations (<100> and <111>) (Right).

Summary

In this study, simulations of a single copper crystal workpiece extrusion through both LTE and NLTE processes were performed for two different initial orientations of workpieces. In this way, a detailed comparative grain refinement performance by using crystal plasticity finite element analysis was addressed. The initial result reveals that the NLTE process has advantages in terms of punching force and deformation distribution. While the LTE process induces strain evolution, increasing from center element to periphery elements, more homogenous plastic strain distribution is examined in the NLTE process. In addition, the orientation distribution of the NLTE process is more homogenous when compared to the LTE process. The SPD analyses were performed under low friction coefficient and backpressure due to the convergence problems of implicit CPFEM UMAT code. For that reason, a more comprehensive analysis will be performed with explicit VUMAT code, and the results will be compared to experimental results as a next step.

References

- [1] R.Z. Valiev, R.K. Islamgaliev, Bulk nan-structured material forms severe plastic deformation, *Prog. Mater. Sci.* 45 (2000) 103-189.
- [2] P.Z Alexander, L.G Langdon, Using high-pressure torsion for metal processing: fundamentals and applications, *Progr. Mater. Sci.* 53 (2008) 893-979. <https://doi.org/10.1016/j.pmatsci.2008.03.002>
- [3] A. Nassef, S. Samy, W.H. El Garaihy, Enhancement of mechanical properties for QAl-Mg-Si alloy using equal channel angular pressing, *World Acad. Sci. Eng. Technol.* 9 (2015) 131-136.
- [4] M. Murashkin, I. Sabirov, D. Prosvirnin, I. Ovid'ko, V. Terentiev, R. Valiev, S. Dobatkin, Fatigue behavior of an ultrafine-grained al-mg-si alloy processed by high-pressure torsion, *Metals* 5 (2015) 578-590. <https://doi.org/10.3390/met5020578>
- [5] Y. Saito, H. Utsunomiya, N. Tsuji, T. Sakai, Novel ultra-high straining process for bulk materials development of the accumulative roll-bonding (arb) process, *Acta Metall.* 47 (1999) 579-583. [https://doi.org/10.1016/S1359-6454\(98\)00365-6](https://doi.org/10.1016/S1359-6454(98)00365-6)
- [6] A. Heczal, F. Akbaripanah, M.A. Salevati, R. Mahmudi, A. Vida, J. Gubicza, A comparative study on the microstructural evolution in am60 alloy processed by ECAP and MDF, *J. Alloy. Compd.* 763 (2018) 629-637. <https://doi.org/10.1016/j.jallcom.2018.06.002>

- [7] Y. Beygelzimer, R. Kulagin, Y. Estrin, L.S. Toth, H.S. Kim, M.I. Latypov, Twist extrusion as a potent tool for obtaining advanced engineering materials: A review, *Adv. Eng. Mater.* 19 (2017) 1- 24. <https://doi.org/10.1002/adem.201600873>
- [8] T. Yalçınkaya, Ü. Şimşek, H. Miyamoto, M. Yuasa, Numerical Analysis of a New Nonlinear Twist Extrusion Process, *Metals* 9 (2019) 1-15. <https://doi.org/10.3390/met9050513>
- [9] S.R. Kalidindi, B.R. Donohue, S. Li, Modeling texture evolution in equal channel angular extrusion using crystal plasticity finite element models, *Int. J. Plast.* 25 (2009) 768-779. <http://doi.org/10.1016/j.ijplas.2008.06.008>
- [10] M.I. Latypov, M. Lee, Y. Beygelzimer, D. Prilepo, Y. Gusar, H.S. Kim, Modeling and characterization of texture evolution in twist extrusion, *Met. Mat. Soc.* 1 (2015) 1-13.
- [11] H. Sheikh, R.Ebrahimi, Modeling the effect of backpressure on dislocation cell structure during simple shear extrusion, *UFGSNM* 17 (2017) 1-9.
- [12] Z. Xu, C. Zhang, K. Wang, K. Zhang, G. Zhao, L. Chen, Crystal plasticity prediction of texture evolution during helical extrusion process of aluminium alloys under three-dimensional deformation path, *J. Alloy. Compd.* 830 (2020) 1-16. <https://doi.org/10.1016/j.jallcom.2020.154598>
- [13] Y. Huang, User-material subroutine incorporating single crystal plasticity in the ABAQUS finite element program, *Mech. Report* 178 (1991).
- [14] T. Yalçınkaya, W. Brekelmans, M. Geers, BCC single crystal plasticity modelling and its experimental identification, *Modell. Simul. Mater. Sci. Eng.* 16 (2008) 1-16. <https://doi.org/10.1088/0965-0393/16/8/085007>
- [15] E.B.W. Schmid, *Plasticity of crystals with special reference to metals*, Hughes & Co, London, 1950.
- [16] D. Peirce, R.J. Asoro, A. Needleman, Material rate dependence and localized deformation in crystalline solids, *Acta Metall.* 31 (1983) 1951-1976. [https://doi.org/10.1016/0001-6160\(83\)90014-7](https://doi.org/10.1016/0001-6160(83)90014-7)
- [17] N. Fang, A new quantitative sensitivity analysis of the flow stress of 18 engineering materials in machining, *J. Eng. Mater. Technol.* 127 (2005) 192-196. <https://doi.org/10.1115/1.1857935>
- [18] H. Yan, X. Zhao, N. Jia, Y. Zheng, T. He, Influence of Shear banding on the formation of brass-type textures in polycrystalline fcc Metals with Low Stacking Fault Energy, *J. Mater. Sci. Technol.* 30 (2014) 408-416. <http://doi.org/10.1016/j.jmst.2013.11.010>
- [19] D. Raabe, F. Roters, Using texture components in crystal plasticity finite element simulations, *Int. J. Plast.* 20 (2004) 339-361. [https://doi.org/10.1016/S0749-6419\(03\)00092-5](https://doi.org/10.1016/S0749-6419(03)00092-5)
- [20] L.A.I. Kestens, H. Pirgazi, Texture formation in metal alloys with cubic crystal structures, *Mater. Sci. Technol.* 32 (2016) 1303-1315. <https://doi.org/10.1080/02670836.2016.1231746>